IEEE Access
Multidisciplinary | Rapid Review | Open Access Journal

Received March 7, 2021, accepted March 25, 2021, date of publication March 29, 2021, date of current version April 7, 2021.

Digital Object Identifier 10.1109/ACCESS.2021.3069293

Control Strategy Research of D-STATCOM Using Active Disturbance Rejection Control Based on Total Disturbance Error Compensation

XUESONG ZHOU, WEIBAO ZHONG, YOUJIE MA, KAIRUI GUO, JIE YIN, AND CONGCONG WEI

Tianjin Key Laboratory for Control Theory & Applications in Complicated Industry Systems, School of Electrical and Electronic Engineering, Tianjin University of Technology, Tianjin 300384, China

Corresponding authors: Weibao Zhong (zwb960920@163.com) and Xuesong Zhou (zxsmyj@126.com)

This work was supported in part by the National Natural Science Foundation of China under Grant 51877152, and in part by the Natural Science Foundation of Tianjin of China under Grant 18JCZDJC97300.

ABSTRACT The distribution static synchronous compensator (D-STATCOM) has the characteristics of nonlinearity, multivariable and strong coupling. Based on the analysis of the D-STATCOM mathematical model, in order to improve the performance of the linear active disturbance rejection controller (LADRC), solve the coupling problem between the d-axis and q-axis current and improve the dynamic tracking response speed and anti-interference ability. A controller with LADRC that compensates the error of the total disturbance is proposed, and the stability of the improved first-order LADRC is proved by the Lyapunov stability theory. Then the output of the full interference channel is corrected to improve the anti-interference ability of the system and the interference observation ability of the linear extended state observer (LESO) to high-frequency noise. Through the analysis of the Bode diagram in the frequency domain, compared with the traditional LADRC, the improved LADRC proposed in this paper has better anti-interference performance. Finally, the improved first-order LADRC is used to replace the traditional D-STATCOM control strategy for current inner loop control, which effectively reduces the disturbance observation error of LESO. The experimental results show that the improved LADRC control performance is better than the proportional integral (PI) controller, and it has better tracking performance and anti-interference performance.

INDEX TERMS Distribution static synchronous compensator (D-STATCOM), total disturbance, linear active disturbance rejection control (LADRC), linear extended state observer (LESO), anti-interference performance.

I. INTRODUCTION

In recent years, due to the large-scale application of smart grids and distributed energy such as wind power and photovoltaics, the grid structure has become more complex. At the same time, the integration of clean energy into the distribution network also poses a huge threat to the stability of the distribution network [1]. In addition, nonlinear power electronic equipment also poses great challenges to the grid structure and the safe operation of the distribution network. The introduction of distribution static synchronous compensator (D-STATCOM) to improve the performance of the distribution network has been used as an economical and effective solution [2], [3]. As a dynamic reactive power compensation device, D-STATCOM can improve system power factor, effectively stabilize voltage, reduce voltage fluctuations and power loss. It is an important device to improve the reliability of power supply and an important part of the field of power quality regulation [4], [5]. Reactive current compensation is related to the tracking control of the compensation current. The tracking control of the compensation current is the key technology of D-STATCOM. Therefore, the AC side current control strategy of D-STATCOM has become a research hotspot [6], [7].

The main method of current loop control is the traditional linear control strategy, which mainly linearizes the system of the nonlinear mathematical model of D-STATCOM. Reference [8] uses proportional integral (PI) controller to decouple

The associate editor coordinating the review of this manuscript and approving it for publication was Tariq Masood.

the system in dq0 synchronous coordinate system. The PI controller has a simple control structure. As long as the parameter design is reasonable, the D-STATCOM with PI controller can achieve satisfactory performance. However, the main disadvantage of the PI controller is that if the operating conditions are different from the assumed conditions, especially in the case of large disturbances such as sudden load changes or short-circuit faults, its control performance will decrease. And due to the increase of external interference, the dynamic characteristics of the PI controller will get worse and worse. Therefore, in view of the deficiencies of PI controllers, many intelligent control methods have been proposed, such as particle swarm [9], neural network [10], fuzzy control [11] and so on.

References [12], [13] use sliding mode control to realize the normal operation of D-STATCOM. Sliding mode control enables D-STATCOM to generate sinusoidal symmetrical grid currents with smaller harmonics to improve the power quality of the grid and provide good performance for the distribution network. [14] proposed a STATCOM control method based on voltage source control, using the traditional DC vector control strategy. But it only affects the voltage fluctuation of the system. [15] proposed an optimal fuzzy control strategy based on robust adaptive PI to control D-STATCOM. The controller can ensure the robustness and stability of the system to external disturbances or the changing uncertainties of the power system. Reference [16] uses genetic algorithm to determine the parameters of PI controller in the research of static var compensator and automatic voltage regulator control system, so that the designed controller has strong robustness. Reference [17] proposed an ant colony algorithm optimization method in order to improve the dynamic performance of STATCOM. The ant colony algorithm fine-tunes the coefficients of the PI controller to realize the optimal dynamic management of STATCOM. Reference [18] proposed a self-tuning PI controller that uses particle swarm optimization technology to adjust the controller gain. This algorithm takes into account the global gain and the adjustment of previous gains, and can obtain the desired gain very effectively. However, because the calculation of the controller gain usually takes a long time, this method is more difficult in practical applications.

The actual D-STATCOM system is a non-linear, strongly coupled, multivariable complex system [19]. The control effect of the traditional control method cannot reach the ideal state, and it is difficult to establish an accurate mathematical model of the controlled system. Therefore, for controlled systems with uncertain factors such as nonlinearity, strong coupling, and multivariate, Professor Han Jingqing proposed Active Disturbance Rejection Control (ADRC) [20], which is widely used in many fields [21]–[24]. ADRC takes the form of the series integrator as the canonical form of the controlled object, takes the unknown dynamics and external disturbances of the system outside the canonical model into total disturbances, and expands the total disturbances of the system into new system state variables [25]. ADRC estimates and compensates the total disturbance of the system in real time through the Extended State Observer (ESO), realizes the dynamic linear feedback, and breaks the boundary between the linear system and the nonlinear system. However, this nonlinear control method faces many parameters and is difficult to adjust, which is not conducive to practical engineering applications.

In order to solve the problems of complex calculation, numerous parameters, and difficulty in parameter adjustment of the nonlinear ADRC, Professor Gao Zhiqiang simplified the structure of the ADRC. In [26], linear active disturbance rejection controller (LADRC) was proposed, and a parameter tuning method based on pole configuration was given. This method attributes the parameter design to the setting of the observer bandwidth and the controller bandwidth, retains the excellent performance of ADRC, simplifies parameter setting, reduces the amount of calculation, and is easy to implement in engineering.

In this paper, based on the theoretical analysis of the second-order LESO observation error, an improved first-order LADRC is proposed to compensate the total disturbance estimation error to improve the dynamic capability of the distribution network during various types of grid defects. The remainder of this paper is organized as follows: Section II is the establishment of the mathematical model of D-STATCOM and an introduction to the traditional first-order LADRC. Section III is the structural design of the improved LADRC, and its stability is proved by the Lyapunov stability theory. According to the frequency domain analysis method, Sections IV and V analyze the anti-interference of the improved LADRC and prove its superiority. Section VI proves that the improved LADRC in the D-STATCOM system can maintain stability. Section VII presents the experimental results, which verify the feasibility and effectiveness of the D-STATCOM system based on the improved LADRC. In Section VIII, some conclusions are summarized. The improved controller can effectively eliminate the oscillations caused by active and reactive power, quickly provide active and reactive power to the power system, better reduce voltage fluctuations caused by the system, and improve the overall efficiency of the distribution network.

II. THE MATHEMATICAL MODEL OF D-STATCOM AND TRADITIONAL LADRC

A. ATHE MATHEMATICAL MODEL OF D-STATCOM

The basic principle of D-STATCOM is to connect the inverter to the AC system in parallel through a filter. By appropriately controlling the switches of the power electronic devices in the inverter, the amplitude and phase of the D-STATCOM input grid current can be adjusted to achieve the purpose of compensating for reactive power [27].

As shown in Fig. 1, the main circuit of D-STATCOM is composed of a voltage-bridge circuit, and its structure is composed of the following parts: voltage support capacitor, which is used to provide a voltage support for the device; The

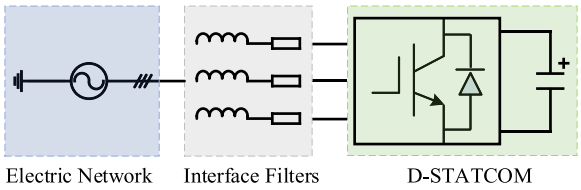

FIGURE 1. Schematic diagram of voltage type D-STATCOM device.

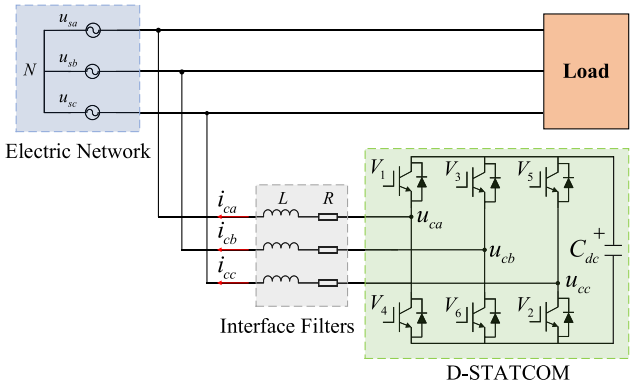

FIGURE 2. Overall control structure of voltage type D-STATCOM device.

voltage source inverter (VSC) is composed of high-power electronic switching devices. It uses space vector pulse width modulation (SVPWM) to control power electronic switches. The DC voltage of the capacitor is converted into an AC voltage of a certain amplitude and frequency; the high-order harmonics in the inverter output voltage can be filtered out by a filter, so that the output voltage of D-STATCOM is close to a sine wave. wave.

The output power quality of D-STATCOM mainly depends on the control performance of the grid-connected inverter. According to the different input modes, D-STATCOM can be divided into voltage source type and current type. Since the input mode of the current source requires a large inductor in series on the DC side to stabilize the DC current, too large series inductance will reduce the response speed of the system. Therefore, voltage source grid-connected inverters are often used in industry.

The overall control structure of the voltage-type D-STATCOM is shown in Fig. 2, where u_{sa}, u_{sb}, u_{sc} represent the three-phase grid voltage; i_{ca}, i_{cb}, i_{cc} are the actual output current of the compensator; u_{ca}, u_{cb}, u_{cc} are the output voltage of the D-STATCOM; u_{dc} is the voltage of the DC side capacitor; R, L are the equivalent resistance and inductance of the filter between the D-STATCOM and the grid connection point.

As shown in Fig. 2, according to circuit law of Kirchhoff, D-STATCOM has the following mathematical relationship in the three-phase coordinate system [15], [28]:

$$L\frac{d}{dt}\begin{bmatrix} i_{ca} \\ i_{cb} \\ i_{cc} \end{bmatrix} = \begin{bmatrix} u_{sa} \\ u_{sb} \\ u_{sc} \end{bmatrix} - R\begin{bmatrix} i_{ca} \\ i_{cb} \\ i_{cc} \end{bmatrix} - \begin{bmatrix} u_{ca} \\ u_{cb} \\ u_{cc} \end{bmatrix} \tag{1}$$

The DC side model is the equation (2):

$$C\frac{du_{dc}}{dt} = s_a i_{ca} + s_b i_{cb} + s_c i_{cc} - \frac{u_{dc}}{R_{dc}} \tag{2}$$

In the above equation, the resistance R_{dc} represents the loss of the capacitor; S_a, S_b, S_c are the switching functions, which are defined as follows:

$$S_k = \begin{cases} 1, & k \text{ phase upper swith is on} \\ 0, & k \text{ phase bottom swith is on} \end{cases} \quad k = a, b, c \tag{3}$$

From equations (1) and (2), it can be seen that the mathematical model in the *abc* coordinate system is more complicated and needs to be simplified for analysis. First, convert the variables of the *abc* coordinate system to the $\alpha\beta$ coordinate system, and the transformation matrix is selected:

$$T_{clarke} = \frac{2}{3}\begin{bmatrix} 1 & -\frac{1}{2} & -\frac{1}{2} \\ 0 & \frac{\sqrt{3}}{2} & -\frac{\sqrt{3}}{2} \end{bmatrix} \tag{4}$$

The AC quantity of the $\alpha\beta$ coordinate system can be converted into the DC quantity of the $dq0$ coordinate system through the park transformation matrix:

$$T_{park} = \frac{2}{3}\begin{bmatrix} \sin\omega t & \cos\omega t \\ -\cos\omega t & \sin\omega t \end{bmatrix} \tag{5}$$

The mathematical model in the $dq0$ coordinate system after Park transformation can be obtained:

$$L\frac{d}{dt}\begin{bmatrix} i_{cd} \\ i_{cq} \end{bmatrix} = -R\begin{bmatrix} i_{cd} \\ i_{cq} \end{bmatrix} + \omega L\begin{bmatrix} i_{cq} \\ -i_{cd} \end{bmatrix} + \begin{bmatrix} u_{sd} \\ u_{sq} \end{bmatrix} - \begin{bmatrix} u_{cd} \\ u_{cq} \end{bmatrix} \tag{6}$$

$$C\frac{du_{dc}}{dt} = \frac{3}{2}(s_d i_{cd} + s_q i_{cq}) - \frac{u_{dc}}{R_{dc}}u_{dc} \tag{7}$$

In equations (6) and (7), u_{sd} and u_{sq} are the voltage components of the d-axis and q-axis on the grid side after coordinate transformation. i_{cd} and i_{cq} are the d-axis and q-axis components of the grid-side current injected by D-STATCOM, respectively. u_{cd} and u_{cq} are the output voltages of D-STATCOM on the d-axis and q-axis. s_d and s_q are the switching function components of the d-axis and q-axis, and ω is the electrical angular velocity (rad/s). So far, the AC model in the *abc* coordinate system has been transformed into the DC model in the synchronously rotating dq0 coordinate system, which is more conducive to control analysis. From equations (6) and (7), we can see that D-STATCOM can be regarded as a first-order system. For measurable first-order systems, the state variables and total disturbances of the system can be observed by designing an appropriate linear extended state observer.

B. STRUCTURAL DESIGN OF D-STATCOM WITH LADRC

The D-STATCOM control system is a double closed loop structure composed of a voltage outer loop and a current inner loop. The outer loop generates d-axis and q-axis reference currents i_{d-ref} and i_{q-ref} to the current inner loop feedback controller [29], [30].

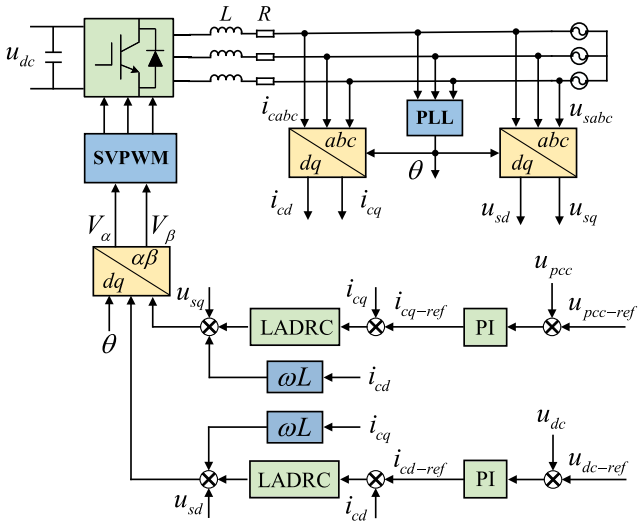

FIGURE 3. Control structure of D-STATCOM with LADRC.

In the outer loop, the capacitor voltage controller obtains the d-axis reference i_{d-ref} through the difference between the expected value and the actual capacitor voltage; the q-axis current reference i_{q-ref} is obtained from the AC system bus voltage or the reactive power controller. The internal current loop controller ensures that the d-axis component i_{cd} of the actual current tracks the d-axis current reference i_{d-ref}; the q-axis component i_{cq} tracks i_{q-ref}. The synchronization between the actual voltage and the voltage of the D-STATCOM is achieved through a phase-locked loop (PLL), and the d-q components of the voltage and current are calculated from the θ obtained by the phase-locked loop. Among them, the reactive power is regulated by the current component i_{cq}, and the active power is regulated by the current component i_{cd}.

Based on the above analysis, this paper designs a double closed loop controller of D-STATCOM system based on LADRC. The controller based on LADRC is used in the current inner loop, and the PI controller is used in the voltage outer loop. The overall structure of D-STATCOM system d-q vector control is shown in Fig. 3.

C. THEORETICAL ANALYSIS OF TRADITIONAL FIRST-ORDER LADRC

LADRC is mainly composed of linear tracking differentiator (LTD), linear extended state observer (LESO) and linear state error feedback control law (LSEF). Among them, LTD is responsible for arranging the transition process and tracking the input signal; LESO can estimate the target state and the total interference of the system; LSEF synthesizes the compensation of disturbance estimator to generate the control signal.

LADRC can equate coupling, uncertainty parameters and external interference to total interference. Among them, LESO is responsible for estimating the total interference and performing pure integral series compensation for the system through dynamic compensation. Then use LESF to transform the integral series system into the desired closed-loop system, and get the desired closed-loop dynamic characteristics.

Since LADRC does not depend on the specific mathematical model of the controlled object, the differential equation of the controlled object can be written in the following general form:

$$\dot{y} = -a_0 y + w + bu \tag{8}$$

In equation (8), u and y are the input and output of the system, respectively; w is the unknown external disturbance; a_0 is the system parameter; b is the unknown input control gain, assuming the estimated value is b_0.

Set $x_1 = y$, define $f(\mathrm{y}, \mathrm{w}) = -a_0 y + w + (b - b_0)u$ as the generalized disturbance of the controlled system, which includes all uncertain factors and unknown external disturbances in the system. Suppose $x_2 = f(\mathrm{y}, \mathrm{w})$, $h = \dot{f}(\mathrm{y}, \mathrm{w})$, the state equation of the system can be written out:

$$\begin{bmatrix} \dot{x}_1 \\ \dot{x}_2 \\ y \end{bmatrix} = \begin{bmatrix} 0 & 1 \\ 0 & 0 \\ 1 & 0 \end{bmatrix} \begin{bmatrix} x_1 \\ x_2 \end{bmatrix} + \begin{bmatrix} b_0 & 0 \\ 0 & 1 \\ 0 & 0 \end{bmatrix} \begin{bmatrix} u \\ h \end{bmatrix} \tag{9}$$

It can be seen from equation (9) that the D-STATCOM system is a first-order controlled object, and x_2 as an expanded new state can be regarded as the sum of unknown disturbances in the system. According to the rank criterion, the system is observable. Thus, according to the equation (9), a second order LESO will be established.

$$\begin{bmatrix} \dot{z}_1 \\ \dot{z}_2 \end{bmatrix} = \begin{bmatrix} -\beta_1 & 1 \\ -\beta_2 & 0 \end{bmatrix} \begin{bmatrix} z_1 \\ z_2 \end{bmatrix} + \begin{bmatrix} b_0 & \beta_1 \\ 0 & \beta_2 \end{bmatrix} \begin{bmatrix} u \\ y \end{bmatrix} \tag{10}$$

In equation (10), z_1 and z_2 track the input signal y and the total disturbance signal, respectively. β_1 and β_2 are the state variables of the observer, and the state variables of the system can be tracked in real time by selecting appropriate parameters.

By extending the state variable z_2, the disturbance compensation link can be designed as follows:

$$u = \frac{-z_2 + u_0}{b_0} \tag{11}$$

When z_2 can accurately track the total disturbance of the system f, the error from z_2 to $f(\mathrm{y}, \mathrm{w})$ can be ignored. Equation (11) can be simplified to:

$$\dot{y} = x_2 + b_0 u = x_2 + (-z_2 + u_0) \approx u_0 \tag{12}$$

The system is a first-order system, and no state differentiation is observed, so LSEF only uses proportional control. The linear state error feedback law of the system can be designed as follows [31]:

$$u_0 = k_p(v - z_1) \tag{13}$$

where k_p is the proportional control gain.

According to equations (12) and (13), the transfer function of the closed-loop system can be obtained:

$$\varphi(s) = \frac{k_p}{s + k_p} = \frac{1}{1/k_p \cdot s + 1} \tag{14}$$

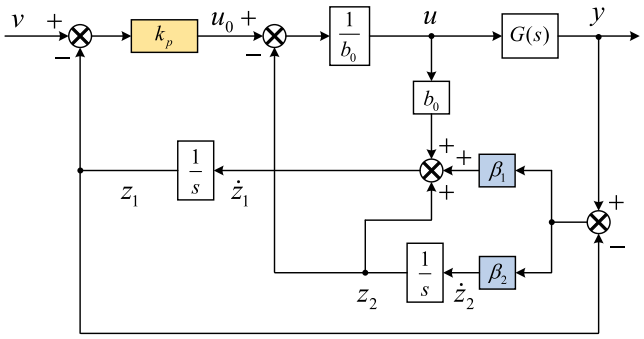

FIGURE 4. Structure diagram of first-order LADRC.

According to equation (14), the bandwidth of proportional control is $\omega_c = k_p$. The larger the parameter ω_c, the faster the dynamic response of the system, but at the same time the stability of the system will also decrease. The system can be stabilized by selecting an appropriate proportional gain.

In order to prevent high-frequency chattering after the system enters a steady state. LADRC only consists of LESO and LSEF, the LADRC of the system represented by equation (8) consists of equations (10), (11), (13). Its structure is shown in Fig. 4:

The LESO parameters can be simplified by the pole configuration method, and the pole configuration is at ω_0, the characteristic polynomial can be obtained as:

$$\lambda(s) = s^2 + \beta_1 s + \beta_2 = (s + \omega_0)^2 \tag{15}$$

The gain of the second-order LESO can be obtained:

$$\beta_1 = 2\omega_0, \beta_2 = \omega_0^2 \tag{16}$$

Therefore, the first-order LADRC can be simplified as the control of the observer bandwidth ω_0 and the controller bandwidth ω_c. Through reasonable adjustment of these two parameters, a better control effect can be obtained.

III. STRUCTURAL DESIGN AND PERFORMANCE ANALYSIS OF IMPROVED FIRST-ORDER LADRC

LESO is the core structure of linear active disturbance rejection technology. The total disturbance can be estimated and compensated by LESO. The controlled system can be converted into a series integrator and controlled, thereby reducing the influence of uncertainty disturbance and improving anti-interference ability of the system. Therefore, it is very important for LESO to estimate the total disturbance without error.

A. ANALYSIS OF IMPROVED CONTROL LAW BASED ON LESO ERROR COMPENSATION

The estimation error of the second-order LESO is defined as:

$$e_1 = z_1 - y, \ e_2 = z_2 - f \tag{17}$$

According to equations (9) and (10), the transfer function from the total disturbance to the estimated error is obtained:

$$\begin{cases} G_{e1}(s) = \dfrac{e_1}{f(s)} = \dfrac{s}{\beta_2 + \beta_1 s + s^2} \\ G_{e2}(s) = \dfrac{e_2}{f(s)} = \dfrac{\beta_1 s + s^2}{\beta_2 + \beta_1 s + s^2} \end{cases} \tag{18}$$

It can be seen from equation (18) that the only influencing factor of the LESO estimation error is the total disturbance f.

Now consider the influence of the tracking error of the total disturbance on the LADRC control performance, and improve the controller. Take the first-order system control law as an example:

$$u = \frac{k_p(v - z_1) - z_2}{b_0} \tag{19}$$

The actual closed-loop system considering the error of LESO estimation is:

$$\begin{aligned} \dot{y} &= f + k_p(v - z_1) - z_2 \\ &= -k_p e_1 - e_2 - k_p y + k_p v \\ &= f + k_p(v - z_1) - z_2 - \bar{E} \\ &= f + b_0 \frac{u_0 - z_2 - \bar{E}}{b_0} \end{aligned} \tag{20}$$

where $\bar{E} = -k_p e_1 - e_2$ is the total error of LESO.

Improved control law can be obtained:

$$u = \frac{k_p(\mathrm{v} - \mathrm{z}_1) - z_2 - \bar{E}}{b_0} \tag{21}$$

In reality, there are many time-varying, nonlinear, strong interference and large inertia industrial control systems. Although LADRC can eliminate the uncertainty of the system to a certain extent, it needs to meet the ideal condition of "the LESO observation error of all states of the system converges quickly in a finite time". Through the above analysis, the LESO observation error is relatively large, and it is difficult to meet the above ideal conditions. Therefore, it is of great practical significance to study the structure optimization of the active disturbance rejection controller, which can reduce the observation error and accurately compensate the external disturbance.

B. COMPENSATION BASED ON TOTAL DISTURBANCE ERROR e_2

Active disturbance rejection control technology uses ESO to estimate the total disturbance in real time, and performs disturbance compensation, so that the object is transformed into an integral series type. Therefore, the uncertainty factor of total disturbance is the key to affecting ESO performance.

From equation (9), the traditional second-order LESO disturbance observation transfer function can be obtained:

$$\frac{z_2(s)}{f(s)} = \frac{\beta_2}{s^2 + \beta_1 s + \beta_2} \tag{22}$$

In the actual control system, only the low frequency signal needs to be paid attention to. Obviously, when ω_0 is large

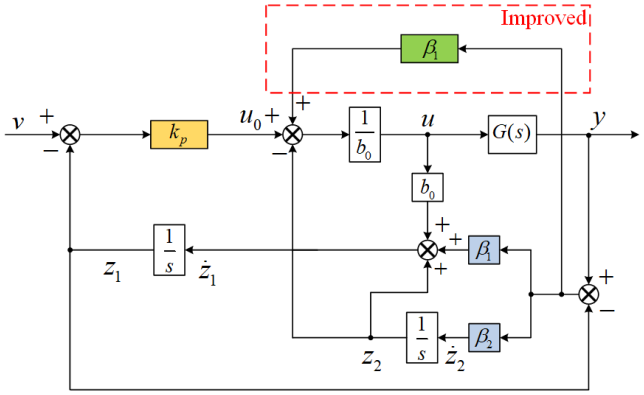

FIGURE 5. Structure diagram of first-order LADRC based on total disturbance compensation.

enough, the middle and low frequency coefficients β_1 and β_2 are obviously greater than 1. Therefore, equation (22) can be approximately equivalent to:

$$\frac{z_2(s)}{f(s)} \approx \frac{\beta_2}{\beta_1 s + \beta_2} \tag{23}$$

Equation (23) performs inverse Laplace transform and combines $\dot{z}_2(s) = -\beta_2 e_1$:

$$f(s) \approx z_2 + \frac{\beta_1}{\beta_2}\dot{z}_2 = z_2 - \beta_1 e_1 \tag{24}$$

Equation (24) is brought into the closed loop system:

$$\dot{y} = u_0 + f - z_2 \approx u_0 - \beta_1 e_1 \tag{25}$$

The compensation term for the estimation error at this time is:

$$\bar{E}_2 = -\beta_1 e_1 \tag{26}$$

The improved LSEF based on compensating the total disturbance is:

$$u = \frac{u_0 - z_2 - \bar{E}_2}{b_0} \tag{27}$$

According to equation (27), the structure diagram of first-order LADRC based on total disturbance compensation is shown in Fig. 5:

C. ANTI-INTERFERENCE TRACKING ANALYSIS OF FIRST-ORDER LADRC BASED ON TOTAL DISTURBANCE ERROR COMPENSATION

After performing Laplace transform of equation (27) and combining equation (10), we can get:

$$u = \frac{k_p(\mathrm{v} - \mathrm{z}_1) - z_2 - \bar{E}_2}{b_0} \tag{28}$$

$$U(s) = \frac{1}{b_0} G_1(s)[\omega_c V(s) - H(s)Y(s)] \tag{29}$$

where:

$$G_1(s) = \frac{(\mathrm{s} + \omega_0)^2}{s^2 + \omega_c s}$$

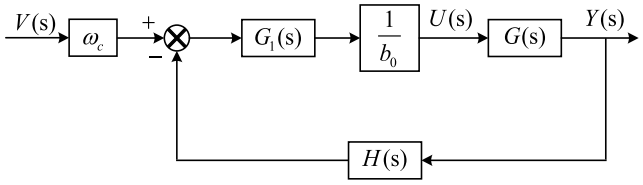

FIGURE 6. Simplified system structure of first-order LADRC based on total disturbance error compensation.

$$H(s) = \frac{2\omega_0 s^2 + (\omega_0^2 + 2\omega_0\omega_c)s + \omega_0^2\omega_0}{(s + \omega_0)^2}$$

According to the above equation, the following simplified block diagram can be obtained:

$$Y(s) = \frac{1}{s}[F(s) + \omega_c V(s)G_1(s) - Y(s)H(s)G_1(s)] \tag{30}$$

Substitute $G_1(s)$ and $H(s)$ into the equation and simplify to get:

$$Y(s) = \frac{s}{(s + \omega_0)^2}F(s) + \frac{\omega_c}{s + \omega_c}V(s) \tag{31}$$

According to equation (31), the output of the system is composed of input and interference. When the output only focuses on the input items, the system control performance is only related to ω_c, not to ω_0. The tracking speed increases with the increase of ω_c, and there will be no overshoot during the tracking process. $f(\mathrm{y}, \mathrm{w})$ contains external disturbance and system internal uncertainties, which is only affected by ω_0. Increasing ω_0 can reduce the low frequency disturbance gain and enhance the system's anti-interference ability. However, the anti-interference of the system is not affected by ω_c, it cannot perfectly reflect the role of ω_c, and cannot achieve the best control quality.

D. STABILITY ANALYSIS OF IMPROVED FIRST-ORDER LADRC

LADRC is a closed-loop system that includes control objects, so there are stability problems. The improved first-order LADRC designed based on the previous article will prove stable in this part.

Take the differential equation of the first-order system represented by equation (8) as an example for analysis. The second-order LESO of the continuous linear system corresponding to equation (9) can be designed as:

$$\begin{cases} \dot{z}_1 = z_2 + \beta_1(\mathrm{y}_1 - \hat{\mathrm{y}}_1) + b_0 u \\ \dot{z}_2 = \beta_2(\mathrm{y}_1 - \hat{\mathrm{y}}_1) + h(\hat{X}, \omega) \\ \hat{y} = z_1 \end{cases} \tag{32}$$

where, $\mathrm{h}(\hat{X}, \omega)$ is the unknown total disturbance observed by LESO. $\hat{\mathrm{y}}_1$ tracking the input signal y.

Assuming $\tilde{\mathrm{y}}_i = y_i - \hat{y}_i$, $i = 1, 2$, $\tilde{\mathrm{y}}_i$ is the direct observation error. The estimated error equation of LESO can be obtained from equations (9), (16) and (32):

$$\begin{cases} \dot{\tilde{\mathrm{y}}}_1 = \tilde{\mathrm{y}}_2 - 2\omega_0\tilde{\mathrm{y}}_1 \\ \dot{\tilde{\mathrm{y}}}_2 = h(X, \omega) - h(\hat{X}, \omega) - \omega_0^2\tilde{\mathrm{y}}_1 \end{cases} \tag{33}$$

$h(X, \omega)$ is the actual value observed by LESO.

Assuming $\varepsilon_j = \frac{\tilde{y}_j}{\omega_0^{j-1}}, j = 1, 2$, ε_j is a scaled estimation error defined in order to analyze the convergence. Equation (33) can be simplified:

$$\dot{\varepsilon}_j = \omega_0 \begin{bmatrix} -2 & 1 \\ -1 & 0 \end{bmatrix} \begin{bmatrix} \varepsilon_1 \\ \varepsilon_2 \end{bmatrix} + \begin{bmatrix} 0 \\ 1 \end{bmatrix} \frac{h(X, \omega) - h(\hat{X}, \omega)}{\omega_0} \quad (34)$$

Let: $A = \begin{bmatrix} -2 & 1 \\ -1 & 0 \end{bmatrix}$, $\mathrm{B} = \begin{bmatrix} 0 \\ 1 \end{bmatrix}$, $\varepsilon = \begin{bmatrix} \varepsilon_1 \\ \varepsilon_2 \end{bmatrix}$

It can be seen from equation (16) that the double pole of LESO is located at ω_0, matrix A is Hurwitz stable, and there is a positive definite Hermitian matrix H that satisfies:

$$A^{\mathrm{T}} H + HA = -I \quad (35)$$

And

$$H = \begin{bmatrix} \frac{1}{2} & -\frac{1}{2} \\ -\frac{1}{2} & \frac{3}{2} \end{bmatrix}$$

Use the Lyapunov function to prove the stability of the controller, which is defined as follows [32]:

$$V(\varepsilon) = \varepsilon^{\mathrm{T}} H \varepsilon \quad (36)$$

There are:

$$\dot{V}(\varepsilon) = \varepsilon^{\mathrm{T}} H \dot{\varepsilon} + \dot{\varepsilon}^{\mathrm{T}} H \varepsilon \quad (37)$$

According to equation (34) and equation (35):

$$\dot{V}(\varepsilon) = -\omega_0(\varepsilon_1^2 + \varepsilon_2^2) + \frac{h(X, \omega) - h(\hat{X}, \omega)}{\omega_0}(-\varepsilon_1 + 3\varepsilon_2) \quad (38)$$

$h(X, \omega)$ satisfies the Lipschitz continuity condition in the definition domain. Therefore, there is a constant c that can meet equation (39):

$$\left|h(X, \omega) - h(\hat{X}, \omega)\right| \le c \left\|X - \hat{X}\right\| \quad (39)$$

In equation (38), $\frac{h(X,\omega)-h(\hat{X},\omega)}{\omega_0}$ satisfies the following equation:

$$\frac{\left|h(X, \omega) - h(\hat{X}, \omega)\right|}{\omega_0}(-\varepsilon_1 + 3\varepsilon_2) \le c(-\varepsilon_1 + 3\varepsilon_2)\frac{\left\|X - \hat{X}\right\|}{\omega_0} \quad (40)$$

According to equations (34) and (38), the following equations can be obtained:

$$-\varepsilon_1 + 3\varepsilon_2 = 2\varepsilon^{\mathrm{T}} HB \quad (41)$$

Equations (40) and (41) can be simplified as:

$$2\varepsilon^{\mathrm{T}} HB\frac{\left|h(X, \omega) - h(\hat{X}, \omega)\right|}{\omega_0} \le 2\varepsilon^{\mathrm{T}} HBc\frac{\left\|X - \hat{X}\right\|}{\omega_0} \quad (42)$$

When $\omega_0 \ge 1$, there is $\frac{\left\|X-\hat{X}\right\|}{\omega_0} = \frac{\left\|\hat{X}\right\|}{\omega_0} \le \left\|\hat{X}\right\|$.

And combined equation (43):

$$\|HBc\|^2 - 2\|HBc\| + 1 \ge 0 \quad (43)$$

Therefore, according to the above equation, equation (44) can be obtained:

$$2\varepsilon^{\mathrm{T}} HB\frac{\left|h(X, \omega) - h(\hat{X}, \omega)\right|}{\omega_0} \le (\|HBc\|^2 + 1)\|\varepsilon\|_1^2 \quad (44)$$

At the same time equation (41) and equation (44) are applied:

$$\dot{V}(\varepsilon) \le -\omega_0(\varepsilon_1^2 + \varepsilon_2^2) + (\|HBc\|^2 + 1)\|\varepsilon\|_1^2 \quad (45)$$

From equation (41), we can see that when $\omega_0 > \|HBc\|^2 + 1$, there are $\dot{V}(\varepsilon) < 0$.

According to Lyapunov's concept of progressive stability, there are:

$$\lim_{t\to\infty} \tilde{y}_i(t) = 0, \quad i = 1, 2 \quad (46)$$

Equation (47) can be obtained according to equations (26) and (27):

$$\begin{aligned} u &= \frac{k_p(\mathrm{v} - \mathrm{z}_1) - z_2 + \beta_1 e_1}{b_0} \\ &= \frac{k_p(\mathrm{v} - \hat{\mathrm{y}}_1) - \hat{y}_2 + \beta_1(\hat{\mathrm{y}}_1 - \mathrm{y}_1)}{b_0} \end{aligned} \quad (47)$$

Let $e = v - y_1$, equation (48) can be obtained by equation (47):

$$u = \frac{k_p(e + \tilde{\mathrm{y}}_1) - (y_2 - \tilde{y}_2) + \beta_1(-\tilde{\mathrm{y}}_1)}{b_0} \quad (48)$$

$$\begin{aligned} \dot{e} &= \dot{v} - \dot{y} = \dot{v} - (\mathrm{y}_2 + b_0 u) \\ &= -k_p(e + \tilde{\mathrm{y}}_1) - \tilde{y}_2 + \beta_1 \tilde{\mathrm{y}}_1 + \dot{v} \end{aligned} \quad (49)$$

To avoid the noise amplification effect of the linear tracking differentiator, the equation (49) is simplified to obtain:

$$\dot{e} = \begin{bmatrix} -k_p \end{bmatrix} e(t) + \begin{bmatrix} -k_p + \beta_1 & -1 \end{bmatrix} \tilde{y}_t \quad (50)$$

$\begin{bmatrix} -k_p \end{bmatrix}$ is Hurwitz stable, because $-k_p$ makes characteristic polynomial $s - k_p$ satisfy Rolls criterion, and it can be obtained from equation (46): $\lim_{t\to\infty} \left\|\begin{bmatrix} -k_p + \beta_1 & -q1 \end{bmatrix}\right\| \tilde{y}_i(t) = 0$, therefore $\lim_{t\to\infty} e_i(t) = 0$. It can be known that the improved first-order LADRC is asymptotically stable, which proves the stability of the improved first-order LADRC according to the theory of Lyapunov's asymptotic stability.

E. INTRODUCTION OF LADRC WITH CORRECTION LINK BASED ON TOTAL DISTURBANCE ERROR COMPENSATION

Through the above analysis of the shortcomings of improved LADRC, to ensure that it can effectively estimate the total disturbance signal, increase the observation bandwidth of LESO and the anti-interference performance of the LADRC. Therefore, referring to the classic control theory, adding the lead-lag correction to the total disturbance can get:

$$\frac{z_2(s)}{f(s)} = \frac{\beta_2}{s^2 + \beta_1 s + \beta_2}\frac{T_e s + 1}{\alpha T_e s + 1} \quad (51)$$

where T_e is the time constant of correction link, α is the coefficient.

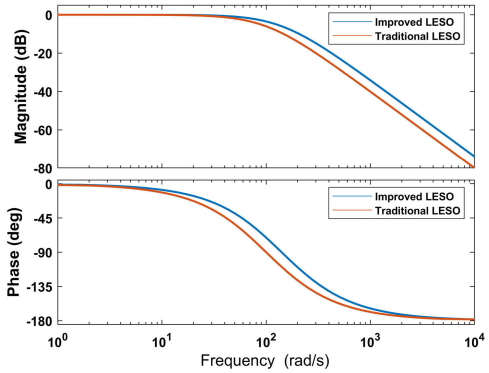

FIGURE 7. Disturbance estimation capability of different LESO.

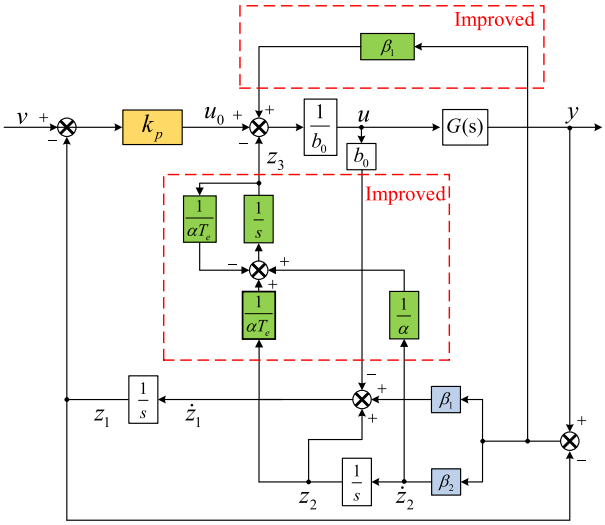

FIGURE 8. The structure of first-order LADRC based on total disturbance error compensation with correction link.

The disturbance estimation capabilities of the two LESOs are shown in Fig. 7. The improved LESO can effectively improve the disturbance observation ability without increasing the observer bandwidth.

From equations (10) and (51), an improved second-order LESO can be obtained:

$$\begin{bmatrix} \dot{z}_1 \\ \dot{z}_2 \\ \dot{z}_3 \end{bmatrix} = \begin{bmatrix} -\beta_1 & 1 & 0 \\ -\beta_2 & 0 & 0 \\ -\beta_2/\alpha & 1/\alpha T_e & -1/\alpha T_e \end{bmatrix} \begin{bmatrix} z_1 \\ z_2 \\ z_3 \end{bmatrix} + \begin{bmatrix} b_0 & \beta_1 & 0 \\ 0 & \beta_2 & 0 \\ 0 & \beta_2/\alpha & 0 \end{bmatrix} \begin{bmatrix} u \\ x_1 \\ x_2 \end{bmatrix} \tag{52}$$

where, z_3 obtained by z_2 through the series correction link is the total disturbance that ultimately acts on the system.

The structure of LADRC with correction link can be obtained from equations (8), (27) and (51), as shown in Fig. 8.

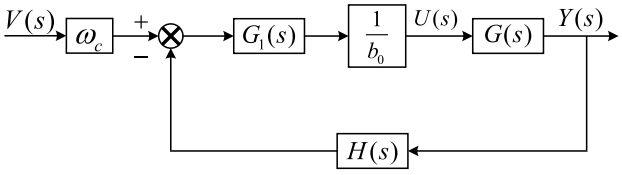

FIGURE 9. Schematic diagram of first-order LADRC based on total disturbance compensation with correction link.

IV. ANALYSIS OF CONVERGENCE AND DISTURBANCE REJECTION OF IMPROVED FIRST-ORDER LADRC

The tracking error of LESO can be defined as: $E_1 = z_1 - y$, $E_2 = z_3 - f$. The tracking error can be reduced by equations (8) and (52):

$$\begin{cases} E_1 = \dfrac{s^2 y}{s^2 + \beta_1 s + \beta_2} - \dfrac{(b_0 s)u}{s^2 + \beta_1 s + \beta_2} \\ E_2 = \dfrac{\alpha T_e s^4 + (2\alpha T_e \omega_0 + 1)s^3}{(\alpha T_e s + 1)(s^2 + \beta_1 s + \beta_2)} \\ \quad + \dfrac{(\alpha T_e \omega_0 + T_e \omega_0 + 2)\omega_0 s^2 + 2\omega_0^2 s}{(\alpha T_e s + 1)(s^2 + \beta_1 s + \beta_2)} \\ \quad - \dfrac{T_e s + 1}{\alpha T_e s + 1} \dfrac{(b_0 \omega_0^2)u}{s^2 + \beta_1 s + \beta_2} \end{cases} \tag{53}$$

Let $y(s) = u(s) = K/s$, where K is a constant, the steady-state error can be obtained:

$$\begin{cases} E_{s1}(s) = \lim\limits_{s \to 0} sE_1(s) = 0 \\ E_{s2}(s) = \lim\limits_{s \to 0} sE_2(s) = 0 \end{cases} \tag{54}$$

Equation (54) shows that LESO has good convergence and can achieve error-free estimation of state variables and total disturbances.

The transfer function can be obtained by equations (28) and (52):

$$U(s) = \frac{1}{b_0} G_1(s)[\omega_c V(s) - H(s)Y(s)] \tag{55}$$

where:

$$G_1(s) = \frac{\alpha T_e s^3 + (1 + 2\alpha T_e \omega_0)s^2 + (2\omega_0 + \alpha T_e \omega_0^2)s + \omega_0^2}{\alpha T_e s^3 + (1 + \alpha T_e \omega_c)s^2 + ((\alpha - 1)T_e \omega_0^2 + \omega_c)s}$$

$$H(s) = \frac{2\alpha T_e \omega_0 s^3 + (2 + T_e \omega_0 + 2\alpha T_e \omega_c)\omega_0 s^2}{\alpha T_e s^3 + (1 + 2\alpha T_e \omega_0)s^2 + (2\omega_0 + \alpha T_e \omega_0^2)s + \omega_0^2} + \frac{(\omega_0 + 2\omega_c + \alpha T_e \omega_0 \omega_c)\omega_0 s + \omega_0^2 \omega_c}{\alpha T_e s^3 + (1 + 2\alpha T_e \omega_0)s^2 + (2\omega_0 + \alpha T_e \omega_0^2)s + \omega_0^2}$$

The following simplified block diagram can be obtained according to the above equation:

According to Fig. 9, the equation (56) can be obtained after Laplace transform equation (8):

$$Y(s) = \frac{1}{s}[F(s) + \omega_c V(s) G_1(s) - Y(s)H(s)G_1(s)] \tag{56}$$

Substituting $G_1(s)$ and $H(s)$ into equation (56), and simplifying it to obtain:

$$Y(s) = \frac{\alpha T_e s^3 + (1 + \alpha T_e \omega_c)s^2 + ((\alpha - 1)\omega_0^2 T_e + \omega_c)s}{(1 + \alpha T_e s)(s + \omega_c)(s + \omega_0)^2} F(s)$$

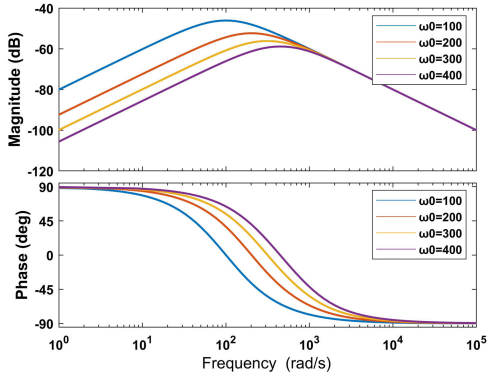

FIGURE 10. Disturbance frequency characteristic curve (ω_0 change).

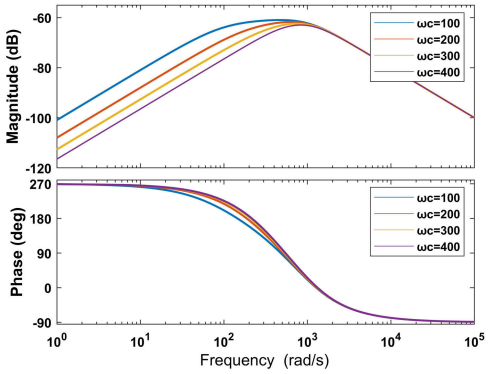

FIGURE 11. Disturbance frequency characteristic curve (ω_c change).

$$+\frac{\omega_c}{s+\omega_c}V(s) \tag{57}$$

The output of the system contains two parts: input and interference, which can be known from equation (57). When the total disturbance f is fully estimated, the system output has only the input items. When the output only focuses on the input items, the system control performance is only related to ω_c, not to ω_0. Tracking speed becomes faster as ω_c increases, and there will be no overshoot during tracking. The tracking ability and anti-interference ability of LESO can be improved by adjusting the bandwidth of the controller, the bandwidth of the observer and the time constant of correction link.

For the improved first-order LADRC, the time constant of calibration link remains unchanged. When $\omega_c = 1000$ and $\omega_0 = 100, 200, 300, 400$ are selected, the frequency characteristic curve as shown in Fig. 10. can be obtained. When $\omega_0 = 1000$ and $\omega_c = 100, 200, 300, 400$ are selected, the frequency characteristic curve is shown in Fig. 11.

It can be seen from Fig. 10 and Fig. 11 that by increasing ω_0 and ω_c, the interference gain can be reduced and the anti-interference ability of the system can be enhanced, indicating that the anti-interference performance of the improved LADRC has been improved.

It can be seen from Fig. 12 that the anti-interference performance of the improved LADRC is better than that of the traditional LADRC. When the time constant of the calibration

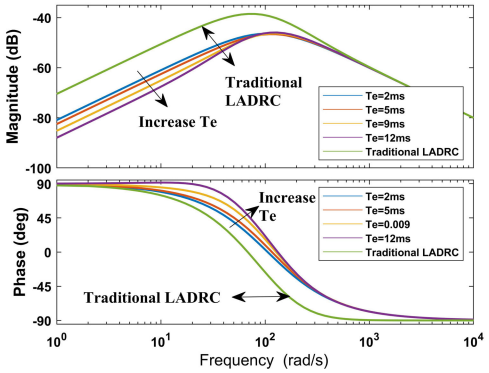

FIGURE 12. Analysis of the influence of the time constant of correction link on the anti-interference characteristics of improved LADRC.

link gradually increases, the anti-interference ability of the improved LADRC gradually increases.

When the disturbance $f(y, w)$ is a unit step signal, the output response of the system can be obtained from equation (57):

$$Y(s) = \frac{\alpha T_e s^3 + (1+\alpha T_e\omega_c)s^2 + ((\alpha-1)\omega_0^2 T_e + \omega_c)s}{(1+\alpha T_e s)(s+\omega_c)(s+\omega_0)^2}\frac{1}{s} \tag{58}$$

The inverse Laplace transform of equation (58) can be obtained:

$$y(t) = d_1 e^{-\frac{1}{\alpha T_e}t} + d_2 e^{-\omega_c t} + (d_3 t + d_4)e^{-\omega_0 t} \tag{59}$$

where:

$$d_1 = -\frac{(\alpha-1)\alpha^2 T_e^3 \omega_0^2}{(\alpha T_e\omega_0 - 1)^2(\alpha T_e\omega_c - 1)}$$

$$d_2 = -\frac{(\alpha-1)T_e\omega_0^2}{(\alpha T_e\omega_c - 1)(\omega_0-\omega_c)^2}$$

$$d_3 = \frac{(2\alpha\omega_0 - \omega_0 - \alpha\omega_c)T_e\omega_0 + \omega_c - \omega_0}{(\alpha T_e\omega_0 - 1)(\omega_0-\omega_c)}$$

$$d_4 = \frac{(1-\alpha-2\alpha T_e\omega_0 + 2\alpha^2 T_e\omega_0 + \alpha T_e\omega_c - \alpha^2 T_e\omega_c)T_e\omega_0^2}{(\alpha T_e\omega_0 - 1)^2(\omega_0-\omega_c)^2}$$

Find the limit of $y(t)$ to know:

$$\lim_{t\to\infty} y(t) = 0 \tag{60}$$

When the external disturbance is a step signal, the steady-state output of the system is zero. Analysis shows that increasing observer bandwidth ω_0 and controller bandwidth ω_c can make $y(t)$ quickly attenuate. The results show that LADRC with improved LSEF and corrective link has strong anti-disturbance ability.

V. ANALYSIS OF ANTI-INTERFERENCE PERFORMANCE OF IMPROVED FIRST-ORDER LADRC IN D-STATCOM SYSTEM

According to Fig. 9, the transfer function of the controlled system can be obtained:

$$G_{c1}(s) = \frac{\omega_c G_1(s)\mathrm{G}(s)/\mathrm{b}_0}{1 + G_1(s)\mathrm{G}(s)H(s)/\mathrm{b}_0} \tag{61}$$

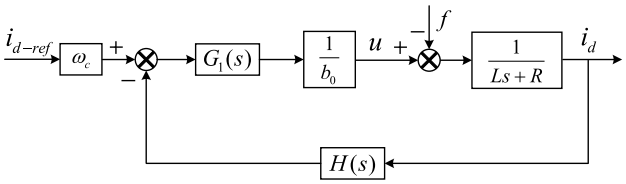

FIGURE 13. D-STATCOM system structure controlled Improved first-order LADRC.

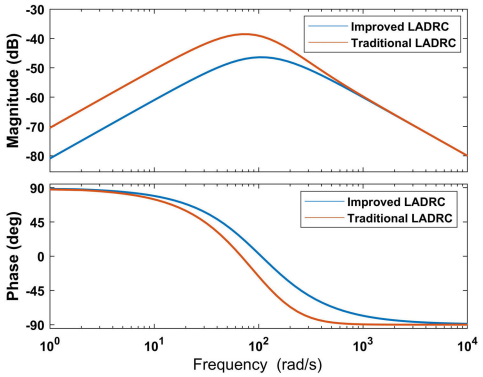

FIGURE 14. Frequency domain characteristics of the improved LADRC and traditional LADRC.

Combining equation (61) and taking the d-axis of the current loop as an example, the D-STATCOM system with the overall structure of the current loop controlled by the improved LADRC is shown in Fig. 13.

$$i_d = \frac{G_1(s)\omega_c}{b_0(Ls+R)+G_1(s)H(s)} i_{d\_ref} - \frac{b_0}{b_0(Ls+R)+G_1(s)H(s)} f = Ci_{d\_ref} + Df \quad (62)$$

where i_d, i_{d_ref}, and f represent the actual output current of the D-STATCOM system, the reference value of the system input current and the total disturbance; C is the transfer function between the actual current output of the system and the given value of the system; D is the transfer function of the disturbance term, which represents the anti-interference performance of the inverter.

From the Bode diagram in Figure 14, the anti-interference ability of the middle and low frequency bands can be compared. The improved LADRC with less disturbance gain is obviously better than the traditional LADRC; in the high frequency band, the two curves roughly coincide. The improved LADRC lags behind the traditional LADRC in phase and increases the interference suppression capability, which can be seen from the phase-frequency characteristics.

VI. STABILITY ANALYSIS OF IMPROVED LADRC IN D-STATCOM SYSTEM

The transfer function of the D-STATCOM system input items can be obtained from equation (62):

$$y = \frac{(1+\alpha T_e s)(s+\omega_0)^2 \omega_c}{a_4 s^4 + a_3 s^3 + a_2 s^2 + a_1 s + a_0} \quad (63)$$

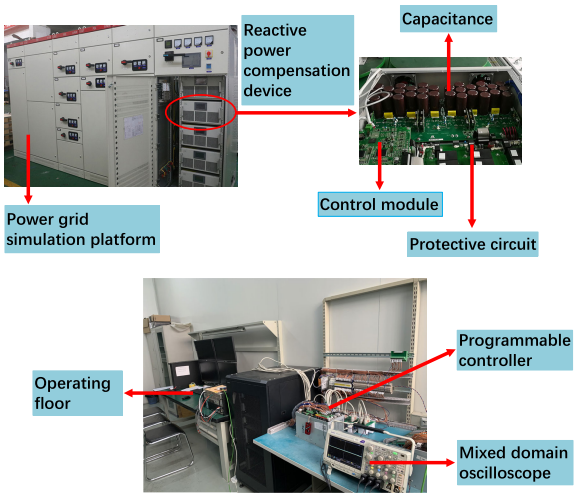

FIGURE 15. Experimental platform of D-STATCOM rated at 20kvar.

Among them:

$$\begin{aligned} a_4 &= \alpha T_e L b_0 \\ a_3 &= L b_0 + \alpha T_e R b_0 + 2\alpha T_e \omega_0 + \alpha T_e L b_0 \omega_c \\ a_2 &= R b_0 + 2\omega_0 + T_e \omega_0^2 + (\alpha - 1) L T_e b_0 \omega_0^2 + L b_0 \omega_c \\ &\quad + \alpha T_e R b_0 \omega_c + 2\alpha T_e \omega_0 \omega_c \\ a_1 &= \omega_0^2 + (\alpha - 1) R T_e b_0 \omega_0^2 + R b_0 \omega_c + 2\omega_0 \omega_c + \alpha T_e \omega_0^2 \omega_c \\ a_0 &= \omega_0^2 \omega_c \end{aligned}$$

It can be seen that $a_i > 0, i = 0, 1, 2, 3, 4$, since the bandwidth of the controller ω_c and the bandwidth of the observer ω_0 are both positive.

The odd Hurwitz determinant is positive, which is a necessary and sufficient condition for system stability. This is known from the stability criterion of Lienard-Chipart algebra.

$$y = \frac{(1+\alpha T_e s)(s+\omega_0)^2 \omega_c}{a_4 s^4 + a_3 s^3 + a_2 s^2 + a_1 s + a_0} \quad (64)$$

where:

$$\Delta_1 = a_1 > 0, \Delta_3 = \begin{vmatrix} a_1 & a_0 & 0 \\ a_3 & a_2 & a_1 \\ 0 & a_4 & a_3 \end{vmatrix} > 0$$

The above analysis shows that the D-STATCOM system combined with the improved first-order LADRC can still remain stable.

VII. EXPERIMENT ANALYSIS

In order to verify the effectiveness of the control strategy designed in this paper, related experiments were carried out on the D-STATCOM rated at 20kvar experimental platform, which is shown in Fig. 15.

Current loop control is an improved active disturbance rejection controller proposed in this paper, and experiments with different working conditions are designed for analysis and verification. The control strategy of D-STATCOM is a double closed loop structure of voltage outer loop and

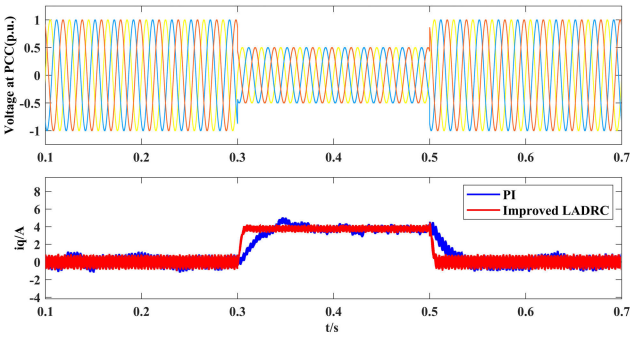

FIGURE 16. Comparison of reactive current tracking curves under the control of PI and improved LADRC under low voltage ride-through.

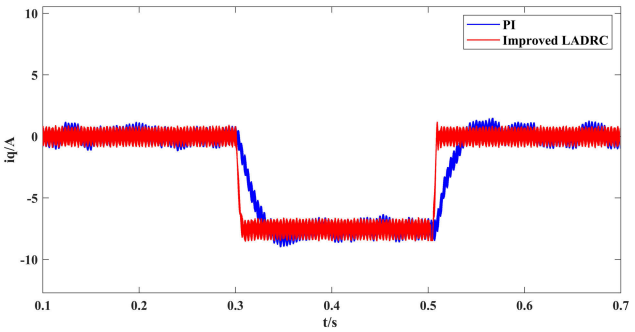

FIGURE 17. Comparison of reactive current tracking under PI and improved LADRC control with increasing and decreasing load.

current inner loop. Because the core of the double closed loop controller designed in this paper is to optimize and improve the inner loop current loop, the improved LADRC is used to control the inner loop. The voltage loop is still the traditional PI controller. Therefore, for experimental verification, experimental analysis under different working conditions compares the control effects of PI and improved LADRC. The parameters in this article are obtained through experience. Appendix A shows the main parameters of the physical parameters, and Appendix B shows the parameters of the controller.

A. ANALYSIS OF REACTIVE CURRENT TRACKING PERFORMANCE

In order to verify the reactive current tracking performance of the improved system, taking the three-phase symmetrical fault of grid voltage and load changes as an example, the tracking performance of reactive current under disturbance is tested.

(I) At $t = 0.3s$, the grid-connected point voltage drops symmetrically to $0.5p.u.$, and is cleared at $t = 0.5s$.

(II) Increase the load by 100% at $t = 0.3s$, and restore the original load at $t = 0.5s$.

1) SCENARIO I

Fig. 16 shows the comparison of reactive current tracking performance between the traditional system and the improved system when the grid voltage has a three-phase symmetrical drop fault. The magnitude of the reactive current tracking fluctuation amplitude and the speed at which the current reaches a steady state after the fluctuation are selected as important reference indicators of the control performance in the two control modes to analyze the anti-interference ability of improved LADRC.

It can be seen from Fig. 16 that when the three-phase voltage drops to 50%, under PI control, the reactive current output by the D-STATCOM fluctuates relatively large, and it takes a long time to reach a stable state. It shows that the PI controller is greatly affected by the voltage drop on the grid side, and its anti-interference performance is relatively low. However, the reactive current fluctuation amplitude under the improved LADRC is relatively small, and it can quickly reach a stable state, indicating that the improved LADRC is less affected by the grid-side voltage fault and has higher anti-interference performance.

2) SCENARIO II

Set the system to increase the load by 100% at $t = 0.3s$, and restore the original load at $t = 0.5s$, which is regarded as system interference. It can be seen from Fig. 17 that, compared with the improved LADRC, the PI controller has a relatively longer adjustment time and a longer time to enter the steady state. The reactive current output by the D-STATCOM fluctuates greatly. The improved LADRC has fast adjustment time, and when the load of the system is increased or decreased, the reactive current tracking performance of D-STATCOM is very good. The comparative analysis shows that the improved LADRC has stronger anti-interference ability.

B. COMPARATIVE ANALYSIS OF D-STATCOM OUTPUT POWER

In order to further verify the anti-interference performance of the improved system, the output power of D-STATCOM under disturbance is tested by taking the three-phase symmetrical fault and load change of the power grid as an example.

(III) At $t = 0.3s$, the grid-connected point voltage drops symmetrically to $0.5p.u.$, and is cleared at $t = 0.5s$.

(IV) Increase the load by 100% at $t = 0.3s$, and restore the original load at $t = 0.5s$.

1) SCENARIO III

Fig. 18 shows the comparison of reactive power and active power output by the traditional system and the improved system when a low voltage ride-through fault occurs in the grid voltage.

Fig. 18 shows that when the three-phase voltage will be 50%, the active power and reactive power output by the D-STATCOM under PI control have relatively large fluctuations, and it takes a long time to reach the stable state of the system. The active power and reactive power output of the D-STATCOM system controlled by the improved LADRC have relatively small fluctuations, and it can quickly reach a stable state. It shows that the improved LADRC is less

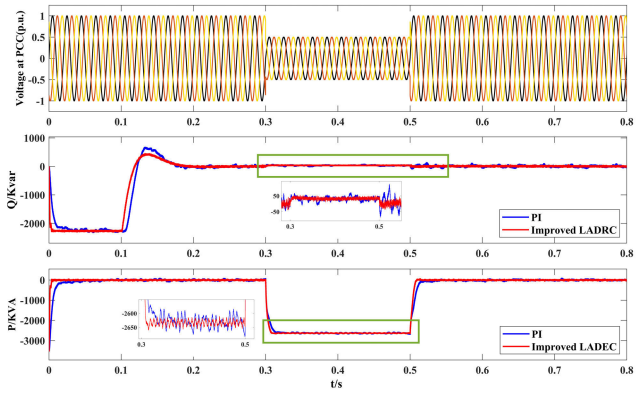

FIGURE 18. Comparison of reactive power and active power under the control of PI and improved LADRC under low voltage ride-through.

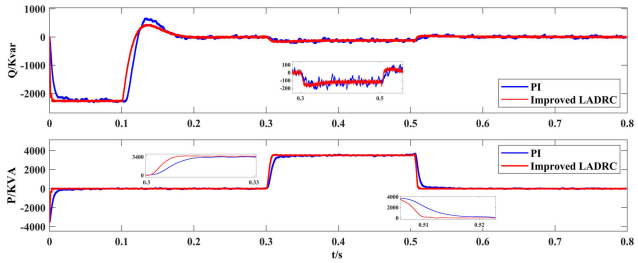

FIGURE 19. Comparison of reactive power and active power under PI and improved LADRC control with increasing and decreasing load.

affected by the grid-side voltage fault and has higher anti-interference performance.

2) SCENARIO IV

Set the system to increase the load by 100% at $t = 0.3s$, and restore the original load at $t = 0.5s$. Fig. 19 shows that the improved LADRC has a faster adjustment time than the PI controller. And when the load is increased and decreased, the reactive power and active power performance of D-STATCOM controlled by the improved LADRC is better.

VIII. CONCLUSION

Aiming at the nonlinear, multivariable and strong coupling characteristics of D-STATCOM, this paper proposes an improved first-order LADRC for the internal current loop of the D-STATCOM system. The key to LADRC performance is whether the extended state observer can accurately estimate the state variables of the system. The innovation of this paper is to propose a linear active disturbance rejection controller that compensates the total disturbance error to improve the control performance of the entire control system. And through the rigorous mathematical derivation of the Lyapunov stability theory, the stability of the improved first-order LADRC is proved, and the asymptotic stability conditions are given. Then correct the output of the total disturbance channel. Finally, the experiment proved the correctness and feasibility of the improved first-order LADRC. In addition, this article only considers the situation of balanced load and symmetrical grid voltage failure. Future work will focus on the study of the D-STATCOM control method of the LADRC under unbalanced load and distorted grid voltage.

TABLE 1. System parameters of D-STATCOM.

Symbol	Quantity	Value	Unit
Q_b	Rated capacity	kvar	20
V_g	Base voltage	V	380
f	Base frequency	Hz	50
u_{dc}	DC-side bus voltage	V	800
C	DC-side bus capacitor	μF	3000
L	Filter output inductance	mH	1
R	Filter output impedance	Ω	0.5

TABLE 2. Controller parameters.

Symbol	Quantity	Unit
ω_c	Controller bandwidth	4000
ω_0	Observer bandwidth	800
b_0	Control gain	11000

APPENDIX A

See Table 1.

APPENDIX B

See Table 2.

REFERENCES

[1] H. Bakir and A. A. Kulaksiz, "Modelling and voltage control of the solar-wind hybrid micro-grid with optimized STATCOM using GA and BFA," *Eng. Sci. Technol., Int. J.*, vol. 23, no. 3, pp. 576–584, Jun. 2020.

[2] S. R. Marjani, V. Talavat, and S. Galvani, "Optimal allocation of D-STATCOM and reconfiguration in radial distribution network using MOPSO algorithm in TOPSIS framework," *Int. Trans. Electr. Energy Syst.*, vol. 29, no. 2, p. e2723, 2019.

[3] S. Rezaeian-Marjani, S. Galvani, V. Talavat, and M. Farhadi-Kangarlu, "Optimal allocation of D-STATCOM in distribution networks including correlated renewable energy sources," *Int. J. Electr. Power Energy Syst.*, vol. 122, Nov. 2020, Art. no. 106178.

[4] R. O. de Sousa, A. F. Cupertino, L. M. F. Morais, and H. A. Pereira, "Minimum voltage control for reliability improvement in modular multilevel cascade converters-based STATCOM," *Microelectron. Rel.*, vol. 110, Jul. 2020, Art. no. 113693.

[5] W. Xiao, J. Li, and Y. Wang, "Study on reactive power compensation strategy based on STATCOM," *Power Capacitor Reactive Power Compensation*, vol. 40, no. 6, pp. 24–29, 2019.

[6] S. N. Duarte, B. C. Souza, P. M. Almeida, L. R. Araujo, and P. G. Barbosa, "Control algorithm for DSTATCOM to compensate consumer-generated negative and zero sequence voltage unbalance," *Int. J. Electr. Power Energy Syst.*, vol. 120, Sep. 2020, Art. no. 105957.

[7] A. Ghias, P. Jose, and V. G. Agelidis, "A novel control method for transformerless H-bridge cascaded STATCOM with star configuration," *IEEE Trans. Power Electron.*, vol. 30, no. 3, pp. 1189–1202, Mar. 2015.

[8] P. Wang, Y. Wang, N. Jiang, and W. Gu, "A comprehensive improved coordinated control strategy for a STATCOM integrated HVDC system with enhanced steady/transient state behaviors," *Int. J. Electr. Power Energy Syst.*, vol. 121, Oct. 2020, Art. no. 106091.

[9] J. Wang and W. Wang, "Self-tuning of PID parameters based on particle swarm optimization," *Control Decis.*, no. 1, pp. 73–76 and 81, 2005.

[10] J. Tang, A. Luo, and K. Zhou, "Variable structure neural network fuzzy control for STATCOM," *J. Hunan Univ., Natural Sci.*, no. 7, pp. 48–52, 2007.

[11] D. Amoozegar, "DSTATCOM modelling for voltage stability with fuzzy logic PI current controller," *Int. J. Electr. Power Energy Syst.*, vol. 76, pp. 129–135, Mar. 2016.
[12] K. D. E. Kerrouche, E. Lodhi, M. B. Kerrouche, L. Wang, F. Zhu, and G. Xiong, "Modeling and design of the improved D-STATCOM control for power distribution grid," *Social Netw. Appl. Sci.*, vol. 2, no. 9, pp. 1–11, Sep. 2020.
[13] A. Halder, N. Pal, and D. Mondal, "Higher order sliding mode STATCOM control for power system stability improvement," *Math. Comput. Simul.*, vol. 177, pp. 244–262, Nov. 2020.
[14] S. Li, L. Xu, and T. A. Haskew, "Control of VSC-based STATCOM using conventional and direct-current vector control strategies," *Int. J. Electr. Power Energy Syst.*, vol. 45, no. 1, pp. 175–186, Feb. 2013.
[15] M. R. Tavana, M.-H. Khooban, and T. Niknam, "Adaptive PI controller to voltage regulation in power systems: STATCOM as a case study," *ISA Trans.*, vol. 66, pp. 325–334, Jan. 2017.
[16] S. Vachirasricirikul, I. Ngamroo, and S. Kaitwanidvilai, "Coordinated SVC and AVR for robust voltage control in a hybrid wind-diesel system," *Energy Convers. Manage.*, vol. 51, no. 12, pp. 2383–2393, 2010.
[17] O. M. Kamel, A. A. Z. Diab, T. D. Do, and M. A. Mossa, "A novel hybrid ant colony-particle swarm optimization techniques based tuning STATCOM for grid code compliance," *IEEE Access*, vol. 8, pp. 41566–41587, 2020.
[18] C.-H. Liu and Y.-Y. Hsu, "Design of a self-tuning PI controller for a STATCOM using particle swarm optimization," *IEEE Trans. Ind. Electron.*, vol. 57, no. 2, pp. 702–715, Feb. 2010.
[19] J. Tang, "Double closed loop control strategy of distribution static synchronous compensator," *High Voltage Eng.*, vol. 36, no. 2, pp. 495–500, 2010.
[20] J. Han, "Auto-disturbances-rejection controller and its applications," *Control Decis.*, no. 1, pp. 19–23, 1998.
[21] Q. Zheng, L. Dong, D. H. Lee, and Z. Gao, "Active disturbance rejection control for MEMS gyroscopes," *IEEE Trans. Control Syst. Technol.*, vol. 17, no. 6, pp. 1432–1438, Nov. 2009.
[22] H. Sira-Ramírez, J. Linares-Flores, C. García-Rodríguez, and M. A. Contreras-Ordaz, "On the control of the permanent magnet synchronous motor: An active disturbance rejection control approach," *IEEE Trans. Control Syst. Technol.*, vol. 22, no. 5, pp. 2056–2063, Sep. 2014.
[23] W. Xue, W. Bai, S. Yang, K. Song, Y. Huang, and H. Xie, "ADRC with adaptive extended state observer and its application to air–fuel ratio control in gasoline engines," *IEEE Trans. Ind. Electron.*, vol. 62, no. 9, pp. 5847–5857, Sep. 2015.
[24] Y. Xia, G. P. Liu, P. Shi, J. Han, and D. Rees, "Active disturbance rejection control for uncertain multivariable systems with time-delay," *IET Control Theory Appl.*, vol. 1, no. 1, pp. 75–81, Jan. 2007.
[25] J. Han, "From PID to active disturbance rejection control," *IEEE Trans. Ind. Electron.*, vol. 56, no. 3, pp. 900–906, Mar. 2009.
[26] Z. Gao, "Scaling and bandwidth-parameterization based controller tuning," in *Proc. Amer. Control Conf.*, 2003, pp. 4989–4996.
[27] K. Sayahi, A. Kadri, F. Bacha, and H. Marzougui, "Implementation of a D-STATCOM control strategy based on direct power control method for grid connected wind turbine," *Int. J. Electr. Power Energy Syst.*, vol. 121, Oct. 2020, Art. no. 106105.
[28] G. He, "Research on control strategy and operation mechanism of D-STATCOM," Guangxi Univ., Liuzhou, China, Tech. Rep., 2019.
[29] R. K. Varma, E. M. Siavashi, S. Mohan, and T. Vanderheide, "First in Canada, night and day field demonstration of a new photovoltaic solar-based flexible AC transmission system (FACTS) device PV-STATCOM for stabilizing critical induction motor," *IEEE Access*, vol. 7, pp. 149479–149492, 2019.
[30] T. Zaveri, B. Bhalja, and N. Zaveri, "Comparison of control strategies for DSTATCOM in three-phase, four-wire distribution system for power quality improvement under various source voltage and load conditions," *Int. J. Electr. Power Energy Syst.*, vol. 43, no. 1, pp. 582–594, Dec. 2012.
[31] D. Yuan, X. J. Ma, Q. H. Zeng, and X. Qiu, "Research on frequency-band characteristics and parameters configuration of linear active disturbance rejection control for second-order systems," *Control Theory Appl.*, vol. 30, no. 12, pp. 1630–1640, Dec. 2013.
[32] Z. Chen, M. Sun, and R. Yang, "On the stability of linear active disturbance rejection control," *ACTA Automatica Sinica*, vol. 39, no. 5, pp. 574–580, 2013.

XUESONG ZHOU received the B.S. degree from the South China University of Technology, Guangzhou, China, in 1984, and the M.S. and Ph.D. degrees from Tsinghua University, Beijing, China, in 1990 and 1993, respectively. From 1993 to 2002, he worked with the School of Electrical and Automation Engineering, Qingdao University, as the Deputy Dean and the Director of the Shandong Provincial Key Laboratory of Power Electronics Engineering. In 1997, he was promoted to a Full Professor. Since 2002, he has been working with the School of Electrical and Electronic Engineering, Tianjin University of Technology, Tianjin, China. His research interests include power system analysis and automation, smart grid, and the field of new energy utilization.

WEIBAO ZHONG received the B.S. degree in electrical engineering and automation from Binzhou University, Shandong, China, in 2019. He is currently pursuing the M.S. degree in electrical and electronic engineering with the Tianjin University of Technology, China. His research interests include reactive power compensation and inverter control technology.

YOUJIE MA received the B.S., M.S., and Ph.D. degrees from Tsinghua University, Beijing, China, in 1984, 1990, and 1993, respectively. From 1993 to 2002, she worked with the School of Electrical and Automation Engineering, Qingdao University, and was promoted to a Full Professor in 1998. Since 2002, she has been working with the School of Automation, Tianjin University of Technology. Her research interests include power system analysis and control, new energy power generation, and power system nonlinear control.

KAIRUI GUO received the B.S. degree in electrical engineering from the Agricultural University of Hebei, Baoding, China, in 2018. She is currently pursuing the M.S. degree in electrical and electronic engineering with the Tianjin University of Technology. Her research interests include grid-connected control of new energy power generation systems and microgrid cyclic current suppression schemes.

JIE YIN received the bachelor's degree in electrical and electronic engineering from the Tianjin University of Technology, in 2018, where he is currently pursuing the master's degree in electrical and electronic engineering. His research interests include smart grid and inverter control technology.

CONGCONG WEI received the B.S. degree from the Department of Information Engineering and Automation, Shanxi Institute of Technology, Yangquan, China, in 2019. He is currently pursuing the M.S. degree with the School of Electrical and Electronic Engineering, Tianjin University of Technology, Tianjin, China. His research interest includes the grid-connected control of new energy power generation systems.